Published in final edited form as:
Ann Otol Rhinol Laryngol. 2008 February ; 117(2): 134–144.

Using Particle Imaging Velocimetry to Measure Anterior-Posterior Velocity Gradients in the Excised Canine Larynx Model

Sid Khosla, MD, **Shanmugam Murugappan, PhD**, **Raghavaraju Lakhamraju, MS**, and **Ephraim Gutmark, PhD**
From the Department of Otolaryngology-Head and Neck Surgery, University of Cincinnati Medical Center (Khosla, Murugappan. Gutmark). and the Department of Aerospace Engineering and Engineering Mechanics. University of Cincinnati (Lakhamraju. Gutmark). Cincinnati. Ohio

Abstract

Objectives—To quantify the anterior-posterior velocity gradient, we studied the velocity flow fields above the vocal folds in both the midcoronal and midsagittal planes. It was also our purpose to use these fields to deduce the mechanisms that cause the anterior-posterior gradient and to determine whether the vortical structures are highly 3-dimensional.

Methods—Using the particle imaging velocimetry method for 5 excised canine larynges. we obtained phase-averaged velocity fields in the midcoronal and midsagittal planes for 30 phases of phonation. The velocity fields were determined synchronously with the vocal fold motion recorded by high-speed videography.

Results—The results show that immediately above the folds, there is no significant anterior-posterior velocity gradient. However, as the flow travels downstream, the laryngeal jet tends to narrow in width and skew toward the anterior commissure. Vortices are seen at the anterior and posterior edges of the flow.

Conclusions—The downstream narrowing in the midsagittal plane is consistent with and is probably due to a phenomenon known as axis switching. Axis switching also involves vortices in the sagittal and coronal planes bending in the axial plane. This results in highly 3-dimensional, complex vortical structures. However, there is remarkable cyclic repeatability of these vortices during a phonation cycle.

Keywords

anterior-posterior velocity gradient; particle imaging velocimetry; phonation. vocal fold; voice production; vortex

INTRODUCTION

How is airflow through the larynx converted into voice? The traditional answer comes from the linear source-filter theory introduced by Fant,[1] in which he proposed that the source of sound is flow modulation produced by vocal fold vibration. According to this theory, the vocal tract acts only as a filter. However, research in the past several years suggests that the airflow through and above the vocal folds may produce additional sources of sounds due to rotational motion in the flow.[2–4] These areas of rotational motion are known as vortices. Vortices can

Correspondence: Sid Khosla. MD, Dept of Otolaryngology-Head and Neck Surgery, University of Cincinnati Medical Center, 231 Albert B. Sabin Way, ML #0528. Cincinnati, OH 42567-0528.

Presented at the meeting of the American Laryngological Association, San Diego, California. April 26–27. 2007.

produce sound by a number of mechanisms, including the interaction of vortices with other vortices or with vocal tract structures (eg, the epiglottis or the pharyngeal wall). Vortices can also break down into chaotic turbulent motion, and this turbulence can produce sound.

Understanding how, and to what degree, these vortices produce sound in the larynx will improve our understanding of voice production, and may result in additional therapies for voice disorders. To determine the acoustic contribution of vortices, the vortical structures first have to be identified. Vortices have been described in mechanical models of the glottis by both flow visualization[5–7] and 2-dimensional particle imaging velocimetry (PIV) techniques.[8–10] Vortices have only recently been identified in an animal model. Using 2-dimensional PIV in an excised canine larynx model, we[11] described 4 types of vortices that occurred during different phases of the phonation cycle; the only plane that was investigated was a coronal plane halfway between the vocal process and the anterior commissure (which we will refer to as the *midmembranous coronal plane).*

If the velocity fields vary in the anterior-posterior direction, the midcoronal plane is not sufficient to describe the 3-dimensional features of the vortices in the laryngeal flow field. Using hot-wire anemometry, previous studies have measured velocities in the anterior-posterior axis of an in vivo canine larynx[12–14] and of an excised canine larynx.[15] In these experiments, a single hot-wire anemometer was used to measure velocity 1 cm above the glottis. Measurements were not made within the first centimeter above the glottis because placement in this location would interfere with vocal fold vibration and might damage the probe tip.[12] All of these studies found that the highest velocities were located anterior and the lowest were posterior, although the exact details of this anterior-posterior velocity gradient differed between investigators. This gradient may not occur at the glottal exit, however, because the velocities were measured 1 cm above the folds. We[11] showed that many vortices originate within the first centimeter above the folds. It is possible that these vortices may cause or accentuate the measured anterior-posterior velocity gradient at 1 cm.

For the canine larynx, hot-wire anemometry does have some limitations that may lead to misinterpretation of the measurements. For example, a single-element hot wire measures the magnitude of the velocity component that is perpendicular to its axis; therefore, it cannot determine the direction of that velocity component within the plane perpendicular to the wire, and this magnitude may not be accurate if there are additional velocity components that are not perpendicular to the measuring element. In addition, the fact that flow reversal cannot be identified[16] makes it impossible to detect or quantify rotational motion.

To detect rotational motion, we use the PIV method, in which micron-size particles or droplets are injected into the flow in order to render it visible when illuminated. Illumination is produced by a laser beam that is spread into a light sheet with a cylindrical lens. The laser is pulsed such that 2 sheets are produced microseconds apart. Both images are recorded on a specialized camera. Computer analysis of the resultant images correlates the particles in the 2 images, allowing a displacement field to be calculated. Because the time between the 2 images is known, a velocity field can be calculated. The advantage of the PIV technique is that it is nonintrusive and can give the magnitude and direction of velocity vectors in any plane of a complex flow field at a given instant of time. In this study, we used PIV to obtain velocity fields in both the midcoronal and midsagittal planes.

To reduce complexity and cost, many computational models of laryngeal airflow and aeroacoustics have assumed that the vortical structures are predominantly 2-dimensional.[17] However, this assumption may significantly mischaracterize the structure and evolution of the vortices. Because vortex-vocal tract interactions will happen in all 3 planes, the assumption of 2-dimensionality will underestimate the acoustic significance of the vortices. Determining the

validity of this assumption is important, because determining the acoustic significance of the vortices is of great clinical interest.

There were 3 main goals of this study. The first was to obtain details of the vortical structures in the midsagittal plane during different phases in the phonation cycle. The second was to quantify the anterior-posterior velocity gradient so that we could determine how, and to what degree, the gradient changes from above the vocal folds to further downstream. By determining the spatial origin and evolution of both the velocity gradient and the vortical structures, it may be possible to determine the mechanisms leading to the velocity gradient. The third goal was to qualitatively determine whether the vortical structures are predominantly 2- or 3-dimensional.

METHODS

In previous articles, we described a method for using PIV in the excised canine larynx during phonation.[11] The techniques are briefly described here. Excised canine larynges were harvested from shared research dogs immediately after the animals were euthanized. The first larynx was from a mongrel dog weighing approximately 16 kg. The membranous folds were approximately 13 mm in length from the vocal process to the anterior commissure. The second and third larynges were from mongrel dogs weighing 22 kg and 20 kg, respectively. The length of the membranous folds was 16.5 mm for the second animal and 15.5 mm for the third one. The fourth and fifth larynges were from mongrel dogs each weighing 17 kg, and the lengths of the membranous folds were 14 mm and 15.5 mm, respectively. Immediately after harvest, each larynx was placed in normal saline solution {0.9% sodium chloride) and refrigerated.

The results shown are all from experiments conducted 1 day after harvest. At this time, all cartilage and soft tissue above the vocal folds were removed. Their removal produced an unobstructed view of the vocal folds. The tracheas were 8 to 10 cm long.

For all animals, the inferior 4 cm of the trachea was placed over a rigid tube (inner diameter of 0.5 inch or 12.7 mm and outer diameter of 0.625 inches or 15.9 mm). To adduct the vocal processes, we placed 1 suture through both vocal processes at the same level. A phonosurgeon placed this stitch with the aid of magnification. The stitch was tied with the minimal tension needed to have a prephonatory width of 0 mm between the vocal processes. Special care was taken to position the suture symmetrically in both the anterior-posterior and inferior-superior directions. The posterior glottis was not closed. There was no noticeable posterior gap for dogs 1, 2, and 3. There was a noticeable posterior gap for dogs 4 and 5. The larynx was fixed in space by use of a square mounting apparatus that had double-prong pins on each side. Each pin was inserted into the cricoid cartilage. The mounting apparatus was connected to a heavy external frame that was bolted to the floor. Electroglottography (EGG) clip electrodes were placed on the soft tissue lateral to the vocal folds on each side. A microphone was placed 1.5 inches (38.1 mm) to the side of the glottal exit in such a way that it did not interfere with laryngeal airflow or with the laser illumination.

The flow that exited the rigid tube and entered the trachea was supplied by a compressor that could produce a steady maximum flow rate of 2,500 cm^3/s at 35 psi. A pressure regulator, a thermocouple, electronic pressure gauges, a mass flowmeter, and an electronic control valve were used to regulate the air upstream. The air was moistened by a humidifier with thermostat control (Conchatherm III, Hudson Respiratory Care. Inc, Temecula, California). The air was then mixed with seeding aerosolized olive oil particles in a settling chamber. The typical particle diameter of the seed was determined previously to be in the range of 10 to 15 μm. A high-speed video camera (High Speed Phantom Works Version 7.1, Vision Research, Wayne, New Jersey) was placed approximately 1 m above the glottal exit in order to visualize vocal

fold vibration. The high-speed images were later analyzed to assess vibratory patterns and to establish the relationship between glottal shape and flow structures.

A 2-dimensional PIV system was used, comprising a frequency-doubled neodymium:yttrium-aluminum-garnet laser with a dual cavity (Solo-PIV, New Wave Research, Fremont, California) integrated with a PIV camera (Imager Intense Camera, LaVision, Ypsilanti, Michigan). The PIV camera and laser were placed in perpendicular axes. The microphone signal was used as a trigger source for acquiring phase-locked PIV images. A fourth-order bandpass with lower and upper cutoff frequencies of 60 and 550 Hz was used to filter the microphone signal. This was then sent into a zero crossing detector that generated a pulse waveform that was 5 V when the signal was above 0 V and was 0 V otherwise. This square waveform was then sent to the PIV hardware as a trigger to obtain images at a particular phase. A total of 30 phases was obtained by varying the delay between the square waveform and the trigger sent t o the PIV hardware. Ten images were acquired at every phase to reconstruct the phase-averaged images over the equivalent of 1 period of the acoustic signal. A data acquisition card was used to record the acoustic, trigger, and EGG signals. The card received a trigger from the high-speed camera that initiates image and signal acquisition. This entire process provided a time correlation between different measurements such as the EGG waveform, the microphone signal, the high-speed image, and the phase-locked PIV vector field.

The laser was focused and spread to produce a laser light sheet in 4 specific planes for all dogs. The first was a coronal plane at the *midmemhranous point,* a position defined to be halfway between the vocal process and the anterior commissure. The second and third were coronal planes 5 mm anterior and 5 mm posterior to the midmembranous point. The fourth plane was a midsagittal view that connected the anterior commissure to the vocal process. For dog 5 only, measurements were also made for an axial cross-sectional view 10 mm above the vocal folds. The thickness of the laser sheet was 1 mm for all of these planes. Rhodamine G powder was placed on the paraglottic tissue and thyroid cartilage to reduce laser light reflections from the wet tissue. The powder never came in contact with the medial aspect of the vocal folds. The camera was then focused to visualize the How in the plane produced by the laser sheet and to give a focused view of the first 10 mm above the glottal exit for all coronal planes and the first 20 mm above the glottal exit for the sagittal plane. The high-speed imaging and PIV measurement for all phases were obtained during 1 phonation trial lasting 3 to 4 minutes. The high-speed video images were taken at a frame rate of approximately 28,000 frames per second. The vocal fold vibration was periodic during the measurement, as evidenced by jitter rates measured over a 20-second period (approximately 4,000 cycles), which ranged from 0.03% to 0.06%.

For all animals, we used the lowest flow rate that produced stable phonation, and a reliable EGG and microphone signal; this resulted in using volumetric flow rates of 350 to 410 cm^3/s.

RESULTS

In a previous article,[11] we reported 4 types of vortices seen in the midmembranous coronal plane: starting vortices seen at the beginning of opening, Kelvin-Helmholtz vortices seen during middle to late opening, entrainment vortices seen at mid-opening, and flow separation vortices seen at middle to end closing. In all 5 dogs studied for this article, we observed these 4 vortices in the anterior, middle, and posterior coronal planes. For each dog, the timing of each type of vortex for each coronal plane was withi in 30° of the other vortices, but it differed from one dog to the other. For example, the flow separation vortex in the anterior plane occurred 24° before the flow separation vortex in the midmembranous plane in dogs 1, 2, and 4. In dogs 3 and 5, the flow separation vortex in the anterior plane occurred 12° after this vortex occurred in the midmembranous plane.

For all 5 dogs, velocity fields in the midsagittal plane were obtained. Figure 1 shows the phase-averaged velocity fields for dog 1 in the midsagittal plane at different phases. One phonation cycle is divided into 360°, and phase-averaged velocity fields were obtained at every 12°. The x-axis connects the anterior commissure to the vocal process and lies in the midsagittal plane. The zero point on the x-axis is the midmembranous point, or the point halfway between the vocal process and the anterior commissure. The anterior direction is to the right. The thick black line represents the line drawn from the anterior commissure to the vocal process. The y-axis is the inferior-superior axis and corresponds to the distance above the vocal folds; the 0 point is at the superior edge of the vocal folds. The length of the arrow and the size of the arrowhead are proportional to the magnitude of the velocity. The contour lines join points of equal vorticity magnitude and are known as isovorticity contours. Vorticity is a measure of rotational motion and has both a magnitude and direction. Only the absolute magnitude of vorticity is represented in these Figures. However, the velocity vectors indicate the direction of rotation; clockwise movement will have a different sign than counterclockwise movement. The closer the isovorticity contours are, the stronger the rotational motion is.

Figure 1A shows the velocity field at 35° (early opening). There is an area of higher flow at about 12 to 20 mm above the folds that was produced in the previous cycle. For the first 5 mm above the folds, the velocity field had low magnitudes and was approximately symmetric around the midmembranous point, with the higher velocities near the most anterior and posterior locations. Figure 1B shows the phase-averaged velocity field at 59°. The flow was increasing both posterior and anterior to the midmembranous point, but the location of the highest velocity was about 2 to 3 mm posterior to the anterior commissure. Figure 1C shows the phase-averaged field at 119°. Directly above the folds, the velocity was about the same for most of the anterior-posterior axis, except at both ends. There was significant vorticity at both the anterior and posterior edges of the flow. Figure 1D shows the phase-averaged field at 165°. Vortices seen more than 5 mm above the folds in Fig 1E have traveled downstream to about 9 to 15 mm above the folds; both of the downstream vortices were entraining fluid such that above 7 mm, the flow was converging. Directly above the folds, the posterior isovorticity contours are bent in the anterior direction. Figure 1E shows the phase-averaged field at 264°. Here the flow converged downstream, but was fairly uniform directly above the folds. The posterior isovorticity contours skewed anteriorly, whereas the anterior isovorticity contours were mostly in the inferior-superior direction. The downstream vorticity seen in Fig 1D traveled downstream and was weakened in Fig 1E. It can be seen that the anterior vortex was entraining some of the glottal flow, causing some flow to skew toward the anterior commissure. Figure 1F shows the velocity field at 300°.

In Fig 1, it can be seen that the flow narrowed, or was convergent downstream for many phases. This behavior can be quantified by measuring the half-width of the jet. which is defined as the distance from the center of the jet to the point at which the velocity drops to 50% of its maximum value. Following methods used in traditional fluid mechanics.[18,19] we used the phase-averaged fields to measure the half-width at certain locations above the folds. When the jet is asymmetric, a half-width is measured for the anterior half, and a half-width is measured for the posterior half; the measurements are then added for a total half-width. Thus, for each chosen point above the folds, there were 30 half-widths corresponding to the 30 phase-averaged fields. The average of these 30 half-widths was then taken. In Fig 2, the averaged half-widths are shown as a function of distance above the folds; it is seen that the jet narrowed, or was convergent, downstream.

From Fig 1, it can be seen that the locations of maximum velocity changed as a function of the distance above the folds. In Fig 3A, the phase-averaged mean (time-averaged) velocity profiles for dog 1 are plotted along the x-axis in the midsagittal plane for different distances above the vocal folds. The only velocity component that is plotted is in the inferior-superior axis. At 3

and 5 mm above the folds, the velocity profile was fairly symmetric above the mid-membranous point; the mean velocity dropped off at both the anterior and posterior ends. At 10 and 15 mm, the highest velocity was just slightly anterior to the midmembranous point. The peak velocity moved further anterior at 20 mm, but was still 3 to 4 mm posterior to the anterior commissure.

The mean axial velocity profiles along the x-axis for dog 2 are shown in Fig 3B. In this case, the velocity decreased significantly from 3 mm to 5 mm above the folds, especially near the vocal process. The maximum mean velocity was anterior for all distances above the fold and moved slightly more anterior for larger downstream distances. The velocity profiles at 3, 5, and 10 mm had a rapid decrease in velocity near the anterior commissure. The analogous plot for dog 3, shown in Fig 3C, looks similar to that in Fig 3A, except for a lower velocity at 6 mm.

In dogs 4 and 5, there was a posterior gap that caused a posterior flow that was relatively constant through most of the cycle. This posterior flow was significantly greater for dog 5 than for dog 4. Figure 3D shows the mean axial velocity profiles for dog 4. The posterior flow probably caused the flow profile to be more symmetric at all distances above the folds. Figure 3E shows the mean axial velocity profile for dog 5; in this case the posterior flow probably caused the maximum velocity to be relatively constant at all measured distances above the fold. Figure 4 shows a phase-averaged velocity field for dog 5 at mid-opening. The posterior flow interacted with the main flow. Because of the arytenoids, we were unable to see the posterior flow below 4 mm above the fold. The velocity fields at other phases (not shown) for dog 5 show that the posterior flow was fairly constant for most phases.

For dog 5, measurements were made in all 3 planes. Figure 5 shows the phase-averaged velocity field in the axial plane 10 mm above the folds at 179°. Z, on the x-axis, refers to a line in the mediallateral direction; the 0,0 x, y point is at the midmembranous point halfway between the medial superior edges of both folds. Figure 5 shows 2 large vortices that were rotating in opposite directions. These axial vortices are hypothesized to be due to axis switching, a phenomenon that has been observed in mechanical jets.

DISCUSSION

Axis switching has been reported in mechanical elliptical[18] and noncircular[19] jets. For these mechanical jets, the major axis of the nozzle was much longer than the minor axis. Therefore, directly downstream of the nozzle exit, the width of the jet in the plane of the major axis was much greater than that in the plane of the minor axis. For some elliptical or other noncircular nozzles in general, the jets in both axes will widen downstream. However, under specific conditions, the jet in the plane of the major axis will narrow while the jet in the plane of the minor axis will widen. At a certain point downstream, the width of the jet in the plane of the minor axis will be greater than that in the major axis. This phenomenon is known as axis switching. In the case of the larynx, the major axis lies in the midsagittal plane and the minor axis lies in the midcoronal plane. The details of axis switching during phonation are described below. First, however, we will compare the anterior-posterior velocity gradients measured by other investigators with our results.

Previous studies in the canine model have used hot-wire anemometry to measure velocities 10 mm above the vocal folds. The majority of these studies have shown higher velocities above the anterior folds. For example, Alipour and Scherer[15] found that in an excised canine larynx, without a vocal tract, the maximum velocities were within a few millimeters posterior to the anterior commissure and the velocity was minimal at the anterior commissure. Berke et al[12] and Bielamowicz et al[13] used an in vivo canine larynx with the vocal tract intact. In both studies[12, 13] the peak particle velocities decreased from anterior to posterior; Bielamowicz et

al[13] found higher velocities at the anterior commissure than did other investigators. Verneuil et al[14] used a 3-probe array with an equal distance between the probes. The probe array was placed in the midsagittal plane such that all probes were 10 mm above the folds. They noted that the instantaneous particle velocities were generally highest at the anterior probe, but reported that this was not always true and that for some trials the instantaneous velocities were actually equal at all 3 probes.

There are several issues to consider when comparing the measurements in the above canine studies to the results reported in this article. The first, most major difference is that we used PIV instead of single-component hot-wire anemometry. The latter technique assumes that all flow is in 1 axis (in these cases, the inferior-superior direction) and that there are no negative velocities. Figure 1 shows that the direction of the velocities in the midsagittal plane can have 2 components. Compared to the midsagittal plane, there was even more rotational motion and flow reversal in the midmembranous coronal planes reported in our previous article[11]; we also see this in the multiple coronal planes used for this study. In Fig 5, it is seen that velocity in the axial plane, 10 mm above the folds, can be significant and will further complicate interpretation of single-component anemometry. The velocity fields in Fig 1 allow determination of the velocities in both the x and y directions at all phases, making the PIV technique more adequate for measuring velocity in the inferior-superior direction than hot-wire anemometry. This is especially true in areas in which there is strong vorticity associated with large velocity gradients.

The differences between single-element hot-wire and PIV measurements may also depend on whether the instantaneous, mean (time-averaged), or peak velocity is measured. Alipour and Scherer[15] have reported that the mean velocities have profiles similar to those of the maximum velocities; although this behavior was seen in dogs 1 and 3, there were significant changes in the velocity profiles for the other dogs. For example, Fig 3B shows the velocity profiles of the mean axial velocity for dog 2. Comparison of these profiles with the maximum axial velocity profiles in Fig 6 shows dramatic differences, especially posterior to the midmembranous points.

The type of canine model also has to be taken into account in interpreting results. To achieve phonation in the in vivo larynx, the recurrent laryngeal nerve is stimulated, whereas adduction sutures are used in the excised canine larynx. The presence of a vocal tract, which will add supraglottal inertance, may also affect the velocity field. Berke et al,[12] Bielamowicz et al,[13] and Verneuil et al[14] all preserved the vocal tract, whereas Alipour and Scherer[15] and our team removed all tissue above the vocal folds. Because of the axis switching phenomenon (discussed below), the addition of a vocal tract may have a greater influence on the velocity fields measured in the coronal plane than on those measured in the sagittal plane.

Although our measured velocity profiles show some general trends, there was also great variability. This variability is probably not due to a difference in vibratory patterns, because similar patterns, in all 5 dogs, were observed from the high-speed video results. There is much greater commonality in comparing flow structures, such as those seen in Fig 1 for dog 1. For dog 1, vortices occurred above the folds at the anterior and posterior edges of the flow; these vortices appeared at about mid-opening. These vortices traveled downstream while new vortices were created above the folds. The downstream vortices entrained fluid, such that the size of the vortices increased as they were convected downstream. From mid-closing to the beginning of opening, stronger vortices were only seen anterior. The exact numbers and sizes of the vortices differed between animals, especially between dogs 1 to 3 and dogs 4 and 5 (due to flow through the posterior gap in dogs 4 and 5), but the general patterns, locations, and timings of the vortices were very similar for all dogs.

One significant similarity is that as mentioned above, the width of the jet decreased downstream in the midsagittal plane from mid-opening to end closing. However, in the coronal plane during closing, the jet diverged, or widened downstream; Khosla et al[11] showed this in detail for the midcoronal plane, but this divergence during closing is also seen in all of the coronal planes for dogs 1 to 5. As mentioned above, the mechanism of axis switching is responsible for jet width spreading in one plane and narrowing in the other plane.

Figure 7 shows the total half-widths for both planes plotted as a function of distance above the folds, for dog 4. When the flows are asymmetric, the half-widths of both sides are summed to give the total half-width. The half-widths are seen to intersect at approximately 7 mm above the fold. Figure 8 shows the half-widths for dogs 1, 3, and 5. Because the vortical structures are more complex in the coronal plane than in the sagittal plane, higher resolution was required in the coronal plane. To obtain higher resolution, we had to have a smaller field of view in the coronal plane, which resulted in measured velocities at greater distances above the vocal folds in the sagittal plane compared to all coronal planes. However, the intersection of the 2 half-width lines, as seen for dog 4, is not necessary to demonstrate axis switching. Instead, the requirement is that as the jet evolves downstream, the half-width in the minor axis increases and the half-width in the major axis decreases. The detailed mechanisms that cause axis switching can be found in the engineering literature[18, 19]; broadly speaking, however, there are 2 main mechanisms of axis switching that are pertinent to the larynx. The first is that the shape and size of the non-axisymmetric nozzle have to meet several rigid criteria. This suggests that there may be certain glottal configurations, seen in laryngeal diseases, that do not produce axis switching. The absence of axis switching may reduce voice quality, as will be discussed below. The second mechanism has to do with the vortices seen in the midsagittal plane.

The vortices at the anterior and posterior edges of the flow are formed by a phenomenon known as Kelvin-Helmholtz instability. This instability is caused by the significant shear stresses at the edges of the jet that are a result of the rapid velocity changes along the sides of the jet, causing the flow to roll up into vortices. These, then, are referred to as Kelvin-Helmholtz vortices. As these vortices travel downstream, the vortices in the sagittal plane will move faster than those in the coronal plane, leading to a phenomenon known as vortex bending. Vortex bending leads to self-induction, which causes the axis switching. For the larynx, this would result in large rotational areas in the axial plane. Indeed, this is seen in Fig 5 for dog 5. The flow emanating from the posterior commissure probably has an effect on the size and shape of the vortices in the axial plane. However, as is seen in Figs 7 and 8, the half-width criterion is met in dogs 4 and 5. The vortices in all 5 dogs are highly 3-dimensional; this finding is in agreement with the theoretical prediction of Mc-Gowan[2] and the work of Neubauer et al[8] and Triep et al.[9]

It is important to note that in each phonation trial the size, phase, and location of the vortices are remarkably consistent, as can be seen by looking at the 10 instantaneous images taken for each phase. If there were significant variation in the shape and location of the vortices, the vortices would be weaker and less coherent than those seen in the instantaneous images. We did not observe this effect. The consistency of the vortices may be important for our ability to produce complex yet consistent voice and speech.

Vortices in the vocal tract will terminate in 2 ways; both are often associated with sound production. The first is that the vortices will break down into turbulent motion, which can produce broadband sound. The second is that the vortices will interact with structures in the vocal tract, such as the pharyngeal wall, the epiglottis, or the base of the tongue; this interaction tends to produce narrowband sound. Axis switching has an influence on the second mechanism, because it causes the jet to spread in the medial-lateral direction (minor axis) rather than the anterior-posterior direction (major axis). The relative acoustic significance of these vortices is

not known. However, 2 characteristics of human voice are complexity and repeatability, characteristics of the vortices described in this work; this similarity suggests that vortices may contribute to voice quality. This work is preliminary, but the findings show the need for further research.

Although planar views can give us an idea of 3-dimensional structures in the flow, 3-dimensional reconstructions (as from computed tomography scans) need to be done; we are presently working on this. We are also planning on conducting experiments to determine how vocal tract structures affect the 3-dimensional vortical structure. In these experiments, the acoustic contribution of the vortical structures will be studied. This work also suggests that careful study be done of the acoustic influence of the flow emanating from the posterior commissure. For applications to voice disorders, we also plan on looking at factors that reduce or inhibit axis switching and that decrease or prevent the organized, complicated structure of the vortices.

CONCLUSIONS

This work shows a highly 3-dimensional, complex vorticity field above the vocal folds during phonation. Directly above the membranous vocal folds, the velocities in the midsagittal plane are relatively constant for most of the phonation cycle. As the flow travels downstream, the jet is seen to narrow in the midsagittal plane, with the maximum velocity located anterior; however, this maximum velocity is always at least 2 mm posterior to the anterior commissure. The combination of jet narrowing in the midsagittal plane and jet widening in the midcoronal plane demonstrates the phenomenon of axis switching. Two types of vortices are consistent with axis switching. The first are vortices at the anterior and posterior edges of the flow in the midsagittal plane, which are due to shear flow instabilities. The second are rotational vortices in the axial plane that result from rotational bending of the vortices in the sagittal and coronal planes. If we draw parallels from the study of jet noise, the large number of highly complex, 3-dimensional, repeatable vortices suggests that these flow structures may produce sources of sound that contribute to voice quality. Now that we have a technique to nonintrusively identify the vortical structures in the canine larynx, research can be done to determine the acoustic contributions of the vortices.

Acknowledgements

Supported by grant 5K08DC005421 from the National Institutes of Health/National Institute on Deafness and Other Communication Disorders. This study was performed in accordance with the PHS Policy on Humane Care and Use of Laboratory Animals, the NIH *Guide for the Care and Use of Laboratory Animals.* and the Animal Welfare Act (7 U.S.C. et seq.); the animal use protocol was approved by the Institutional Animal Care and Use Committee (IACUC) of the University of Cincinnati.

References

1. Fant, G. Acoustic theory of speech production. The Hague, the Netherlands: Moulton; 1950.
2. McGowan RS. An aeroacoustic approach to phonation. J Acoust Soc Am 1988;83:696–704. [PubMed: 3351128]
3. Shadle CH, Barney A, Davies POAL. Fluid flow in a dynamic mechanical model of the vocal folds and tract: II. Implications for speech production studies. J Acoust Soc Am 1999;105:456–66.
4. Kucinschi BR, Scherer RC, DeWitt KJ, Ng TTM. Flow visualization and acoustic consequences of the air moving through a static model of the human larynx. J Biomech Eng 2006;128:380–90. [PubMed: 16706587]
5. Shadle, CH.; Barney, AM.; Thomas, DW. An investigation into the acoustics and aerodynamics of the larynx. In: Gauffin, J.; Hammarberg, B., editors. Vocal fold physiology. San Diego, Calif: Singular; 1991. p. 73-82.

6. Pelorson X, Hirschberg A, Van Hassel RR, Wijnands APJ. Theoretical and experimental study of quasisteady-flow separation within the glottis during phonation. Application to a modified two-mass model. J Acoust Soc Am 1994;96:3416–31.
7. Kucinschi BR, Scherer RC, DeWitt KJ, Ng TTM. An experimental analysis of the pressures and flows within a driven mechanical model of phonation. J Acoust Soc Am 2006;119:3011–21. [PubMed: 16708957]
8. Neubauer J, Zhang Z, Miraghaie R, Berry DA. Coherent structures of the near field flow in a self-oscillating physical model of the vocal folds. J Acoust Soc Am 2007;121:1102–18. [PubMed: 17348532]
9. Triep M, Brucker C, Schroder W. High-speed PIV measurements of the flow downstream of a dynamic mechanical model of the human vocal folds. Exp Fluids 2005;39:232–45.
10. Erath BD, Plesniak MW. An investigation of bimodal jet trajectory in flow through scaled models of the human vocal tract. Exp Fluids 2006;40:683–96.
11. Khosla SM, Murugappan S, Gutmark E, Scherer R. Vortical flow field during phonation in an excised canine larynx model. Ann Otol Rhinol Laryngol 2007;116:217–28. [PubMed: 17419527]
12. Berke GS, Moore DM, Monkewitz PA, Hanson DG, Gerratt BR. A preliminary study of velocity during phonation in an in vivo canine model. J Voice 1989;3:306–13.
13. Bielamowicz S, Berke GS, Kreiman J, Gerratt BR. Exit jet particle velocity in the in vivo canine laryngeal model with variable nerve stimulation. J Voice 1999;13:153–60. [PubMed: 10442746]
14. Verneuil A, Berry DA, Kreiman J, Gerratt BR, Ye M, Berke GS. Modeling measured glottal volume velocity waveforms. Ann Otol Rhinol Laryngol 2003;112:120–31. [PubMed: 12597284]
15. Alipour F, Scherer RC. Pulsatile airflow during phonation: an excised larynx model. J Acoust Soc Am 1995;97:1241–8. [PubMed: 7876445]
16. Mueller, TJ. Flow visualization by direct injection. In: Goldstein, RJ., editor. Fluid mechanics measurements. Washington, DC: Taylor & Francis; 1996. p. 367-450.
17. Zhao W, Zhang C, Frankel SH, Mongeau L. Computational aeroacoustics of phonation, part I: Computational methods and sound generation mechanisms. J Acoust Soc Am 2002;112:2134–46. [PubMed: 12430825]
18. Ho CM, Gutmark E. Vortex induction and mass entrainment in a small-aspect-ratio elliptic jet. J Fluid Mech 1987;179:383–405.
19. Gutmark EJ, Grinstein FF. Flow control with noncircular jets. Annu Rev Fluid Mech 1999;31:239–72.

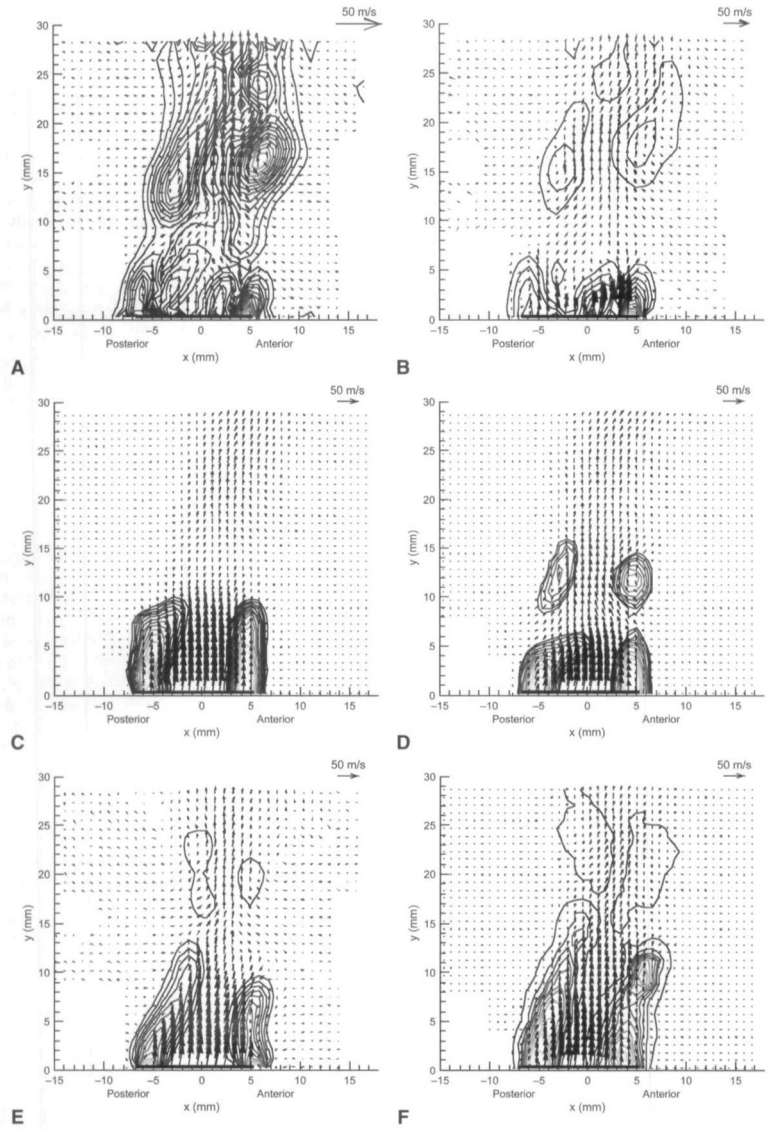

Fig 1.

Phase-averaged velocity field for dog 1. x-Axis refers to line that passes through anterior commissure and vocal process. Thick, dark line on x-axis connects vocal process to anterior commissure. y-Axis represents distance above superior edge of vocal folds. Rotational lines join vectors of equal vorticity. The closer the lines are together, the stronger the velocity is. **A**-**F** show similar fields for dog 1 at different phases; **A**) 35°; **B**) 59°; **C**) 119°; **D**) 165°; **E**) 264°; **F**) 300°.

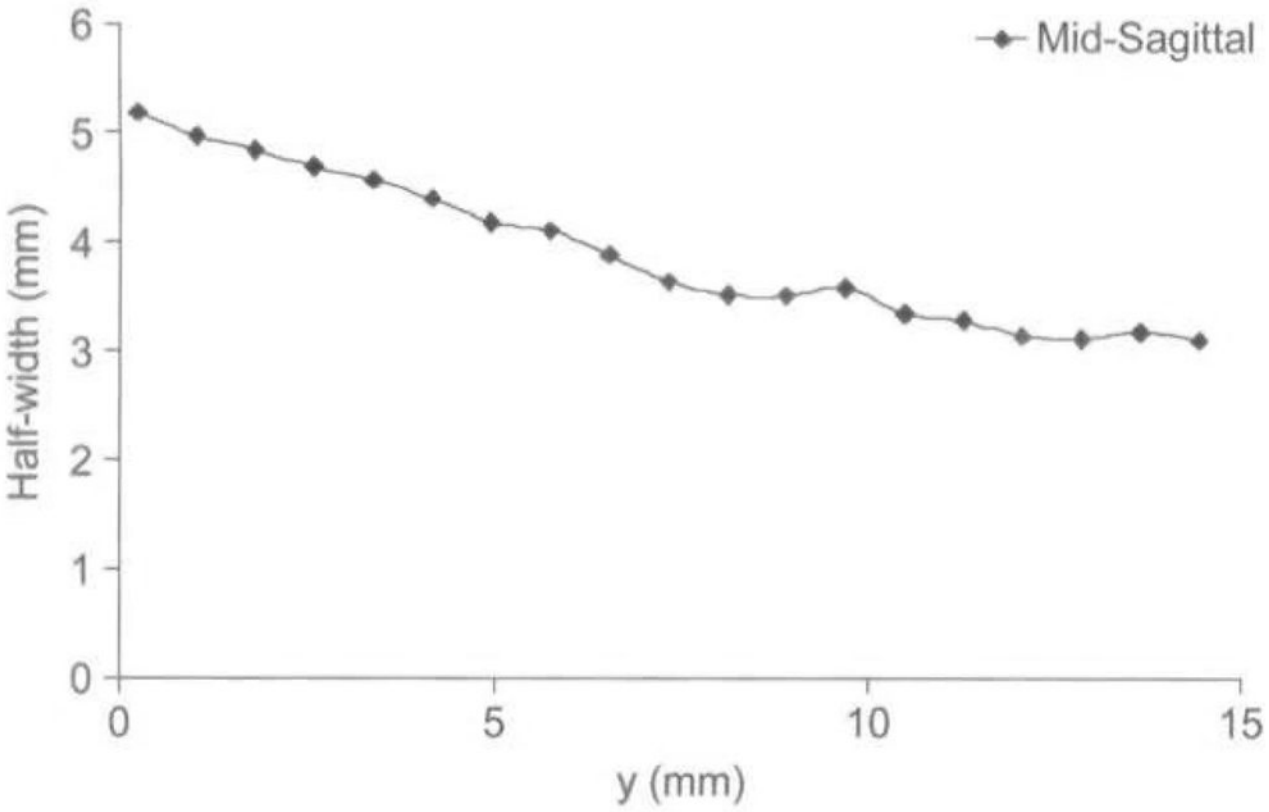

Fig 2.
Jet half-width plotted for distances downstream for dog 1 in midsagittal plane.

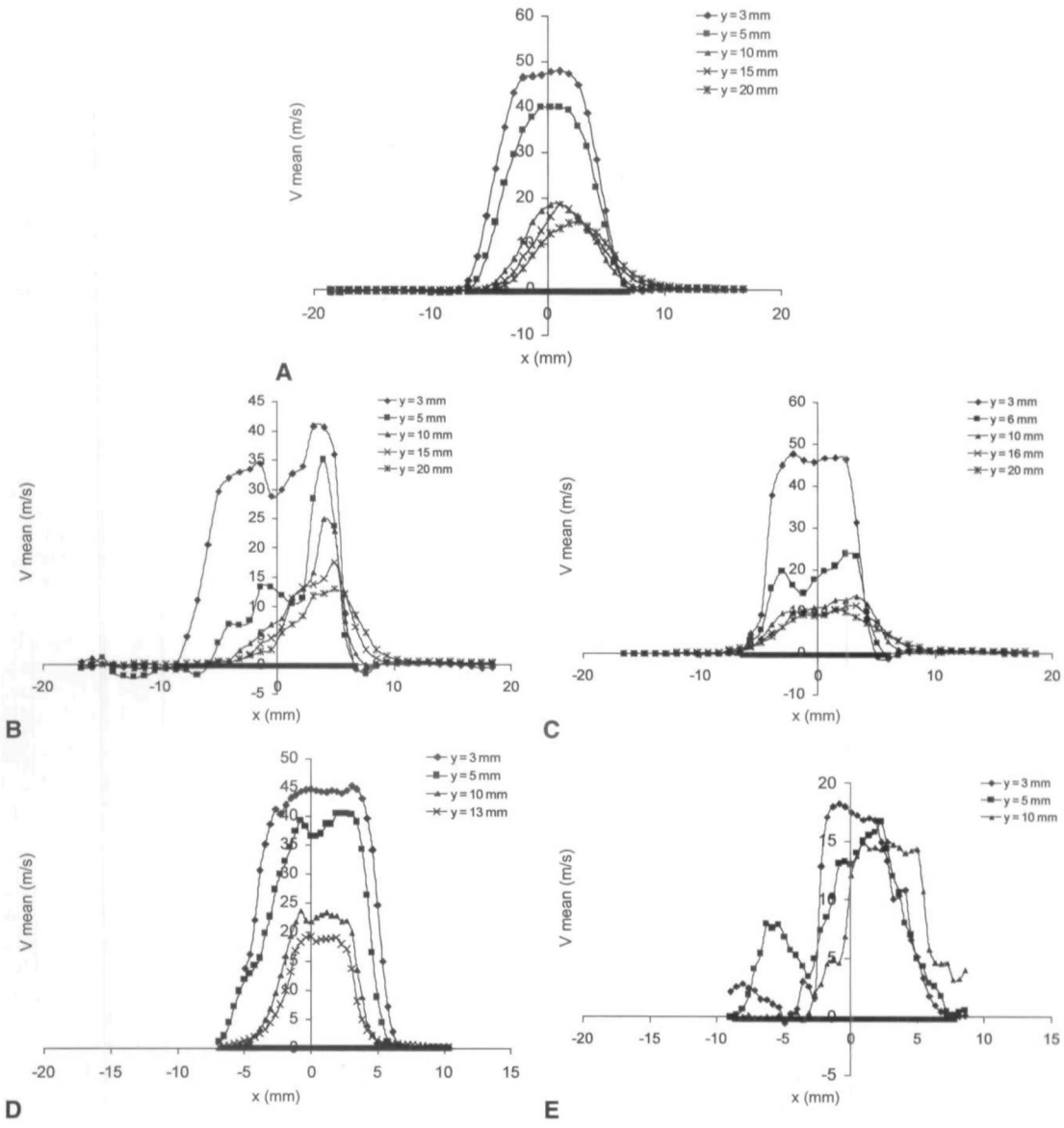

Fig 3.

Time-averaged mean velocity plotted as function of location on anterior-posterior axis at different locations downstream for **A**) dog 1; **B**) dog 2; **C**) dog 3; **D**) dog 4; and **E**) dog 5.

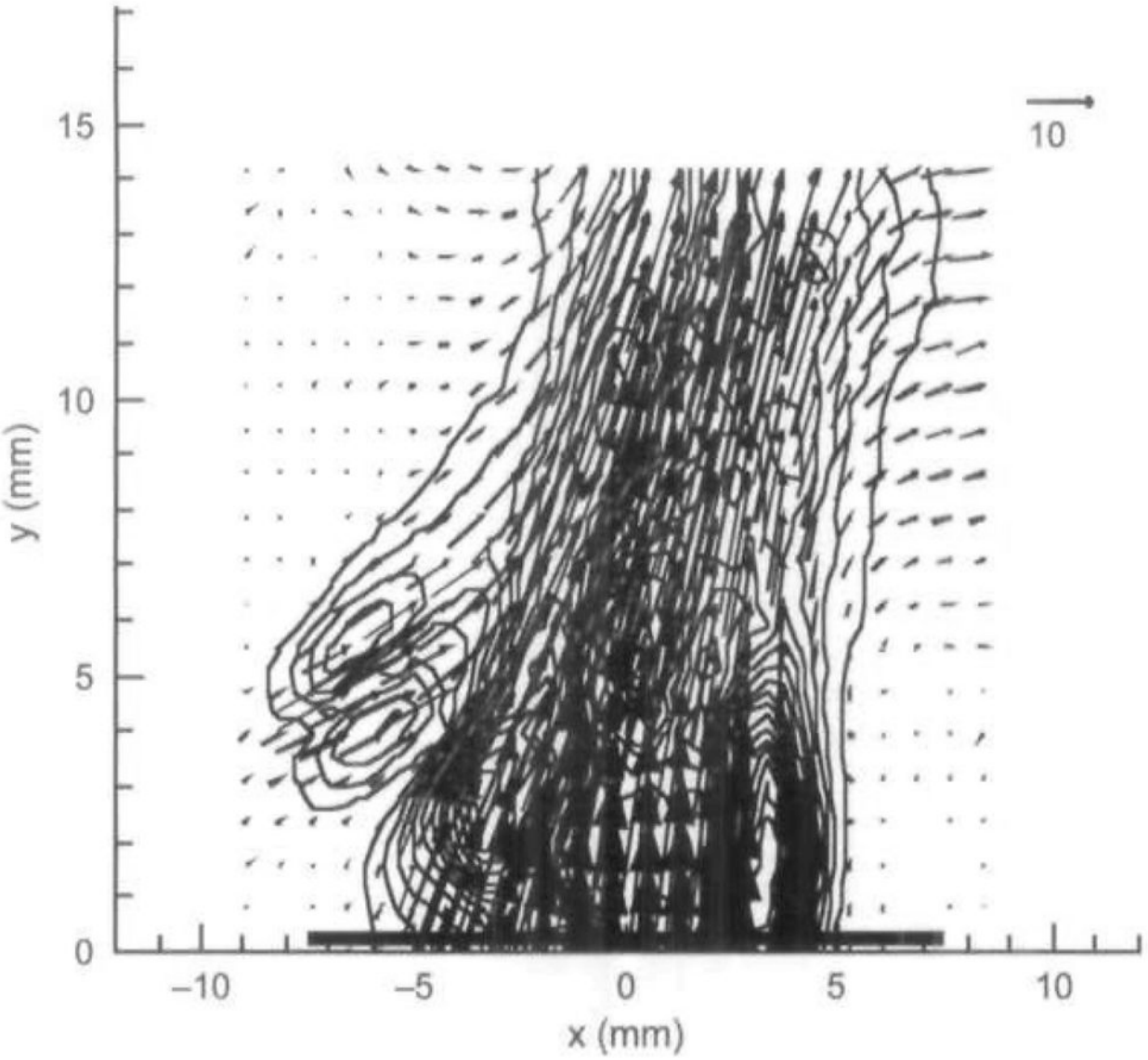

Fig 4.
Phase-averaged velocity field in midsagittal plane for dog 5 at mid-opening. Flow from posterior gap can be seen along posterior edge.

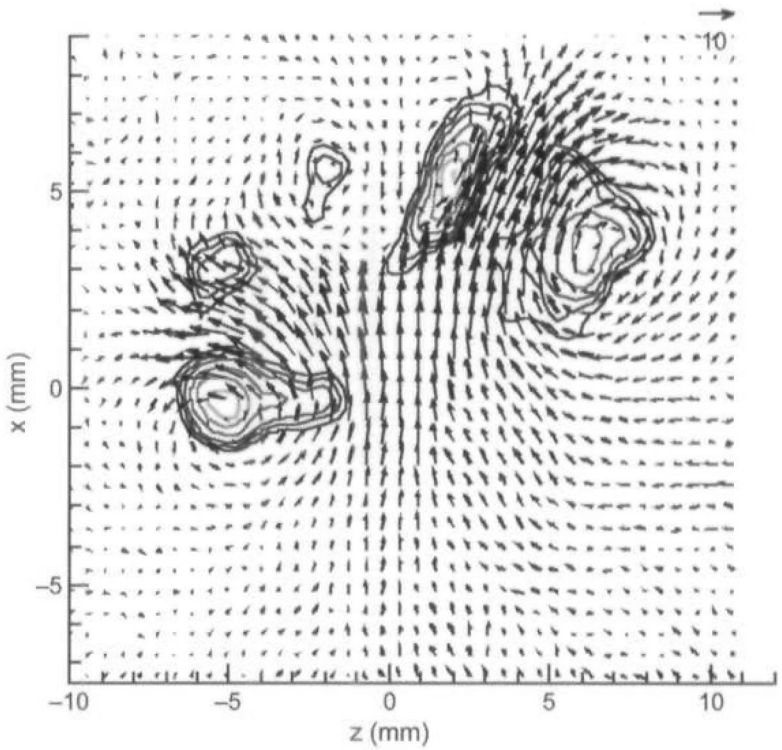

Fig 5.

Phase-averaged velocity field in axial plane 10 mm above superior edge of vocal fold. X, on y-axis, refers to distance in anterior-posterior direction, with 0 representing midmembranous point. Z, on x-axis, is distance in medial-lateral direction, with 0 representing point halfway between superior-medial edges of right and left folds. This is for mid-opening. Large vortex over each fold can be seen.

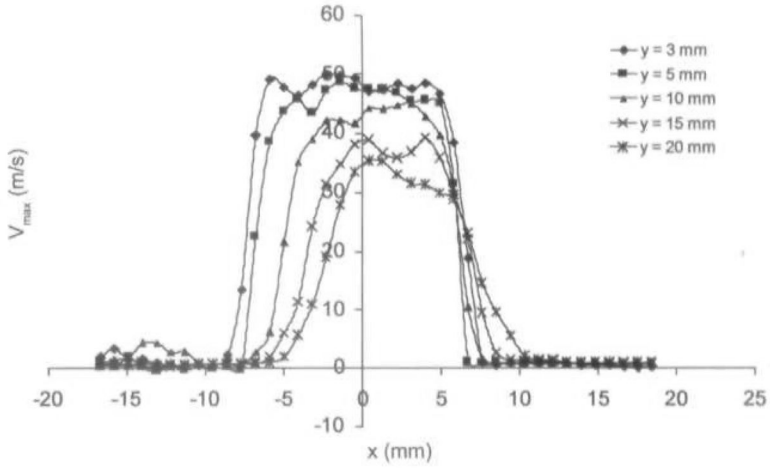

Fig 6.

Velocity profile for dog 2. This is similar to Fig 3. except that averaged maximum velocity is plotted on y-axis, instead of mean velocity used in Fig 3.

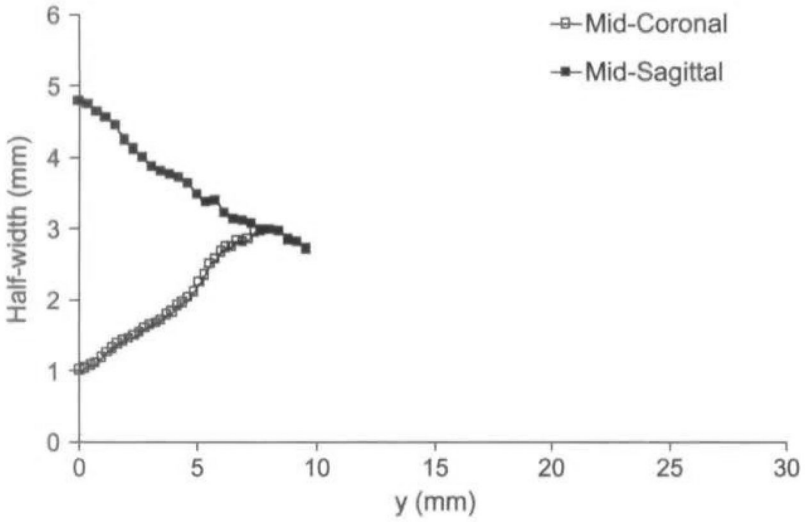

Fig 7.

Averaged half-width plotted as function of distance above vocal folds for dog 4 in both midsagittal and mid-coronal planes. It can be seen that half-width in midsagittal plane decreases and half-width in midcoronal plane increases. Two lines intersect at about 7 mm above folds. Similar half-width plots are shown in Fig 8.

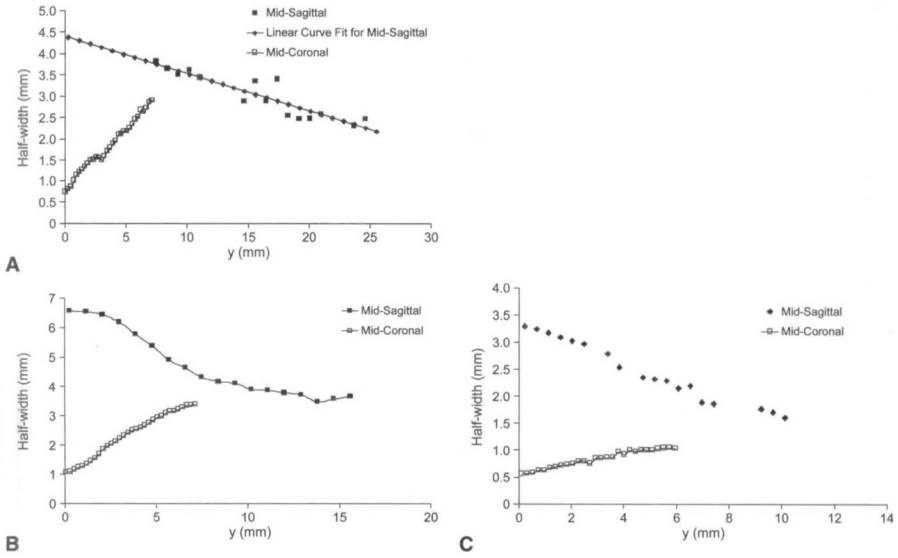

Fig 8.
Half-width plots for **A**) dog 1; **B**) dog 3; and **C**) dog 5.